

Experiments on cylinder wake stabilization in an electrolyte solution by means of electromagnetic forces localized on the cylinder surface

T. Weier, G. Gerbeth, G. Mutschke, E. Platacis[†] & O. Lielausis[†]

*Research Center Rossendorf Inc.,
PO Box 51 01 19, D-01314 Dresden, GERMANY
Tel.: +49-351-260-2373, Fax: +49-351-260-2007
email: weier@fz-rossendorf.de*

[†] *Institute of Physics Riga, LATVIA*

Abstract

Electromagnetic body forces, i.e. Lorentz forces, have been used to modify the boundary layer around a circular cylinder in cross flow. Depending on the polarity of the applied electric field different effects on the flow can be obtained. Lorentz forces directed with the mean flow are able to prevent the boundary layer from separation. Therefore flow separation as well as the von Kármán vortex trail can be suppressed. When the momentum gain produced by the Lorentz forces in the boundary layer is high enough, thrust is produced, what results in a jet flow originated from the cylinders back side. If the Lorentz forces are directed opposite to the mean flow, the separation points are shifted towards the front stagnation point, the recirculation region broadens and the von Kármán vortex trail is modified. The described technique gives a variety of opportunities to control the flow around the cylinder and the flow structure of the cylinder wake. Results from flow visualizations and numerical calculations are presented.

Keywords: body force, boundary layer, cylinder wake, flow control, flow separation, MHD

1 Introduction

Specific possibilities for flow control exist if the considered fluid has a non-zero electrical conductivity. In that case the application of suitable magnetic fields and/or external electric currents allows to organize a volume force distribution inside the fluid. To some extent this force distribution can be

adapted to the desired action of the electromagnetic forces by suitably arranging the magnetic and/or electric fields. The electromagnetic body force or Lorentz force \mathbf{F} results from the vector product of the current density \mathbf{j} and the magnetic induction \mathbf{B}

$$\mathbf{F} = \mathbf{j} \times \mathbf{B}. \quad (1)$$

The current density \mathbf{j} is given by Ohm's law:

$$\mathbf{j} = \sigma(\mathbf{E} + \mathbf{U} \times \mathbf{B}), \quad (2)$$

where \mathbf{E} denotes the electric field, \mathbf{U} the velocity, and σ the electrical conductivity, respectively. Obviously, the electromagnetic body force can be generated by the application of either a magnetic field alone, or by a combination of magnetic and electric fields. If the conductivity of the considered fluid is high ($\sigma \sim 10^6$ S/m) as in the case of liquid metals or semiconductor melts, already an external magnetic field alone can have a strong influence on the flow. Interaction of this external magnetic field with the mean fluid flow causes electrical currents as described by the second term of the right hand side of Eq. (2). These induced currents together with the external magnetic field generate the Lorentz force. Some typical magnetohydrodynamic (MHD) effects for such high-conducting liquids are described in another paper of this volume [1].

In the present paper we focus on some magnetohydrodynamic effects in low conducting fluids ($\sigma \sim 10$ S/m) like seawater or electrolytes. In that case the electrical currents originating from $\mathbf{j} = \sigma(\mathbf{U} \times \mathbf{B})$ are generally much too low to produce any noticeable effect on the flow even for magnetic fields of several Tesla. Therefore, one has to apply a separate external field \mathbf{E} in order to produce a sufficient electrical current density in the fluid, necessary for the desired fluid flow control. To achieve a specific goal, one has to choose the appropriate configuration of external magnetic and electric fields yielding some optimal Lorentz force distribution. Electrical currents fed via electrodes to a low-conducting fluid will only slightly penetrate into the liquid. Therefore, one can assume that the Lorentz force will be noticeable only in some vicinity of the electrodes, i.e. at the surface of the body. One can estimate from these rough considerations that such electromagnetic forces will be effective mainly for boundary layer flows, but not much for bulk fluid flows.

One example of applying Lorentz forces to sea water flows is the recent R&D on MHD ship propulsion [2], practically realized with the Japanese ship YAMATO-1 [3]. However, the efficiency of such a MHD-thruster is still rather low. The thruster needs to act on a large fluid volume to produce a necessary amount of thrust to drive the ship. This represents a difficult task for magnetic field construction, and even modern superconducting magnets cannot provide sufficient magnetic field strength over such large volumes.

The electric and magnetic fields may vary in space and time and so produce an easy changeable force which can be precisely adjusted to achieve a specific goal. No mechanically moving parts are needed to induce this varying force, therefore there is no reason for additional attrition. However, one is confronted with electrochemistry processes at the electrodes generally resulting in the occurrence of electrolytical bubbles.

The idea to influence a low-conducting boundary layer flow by electromagnetic forces dates back to the 60's [4, 5]. Recently these ideas received new attention to control turbulent boundary layers [6, 7], and to be used for seawater ships or submarines.

2 Transition Delay of a laminar boundary layer on a flat plate

An instructive example to explain the general idea of boundary layer control by means of electromagnetic forces is the case of a flat plate with a Lorentz force applied in the streamwise direction.

Figure 1 shows a schematic view of the field configurations to induce a streamwise directed Lorentz force. The velocity, magnetic and electric fields can be written as

$$\mathbf{U} = (U_x, U_y, 0)^T, \quad \mathbf{E} = (0, E_y, E_z)^T, \quad \mathbf{B} = (0, B_y, B_z)^T. \quad (3)$$

The low electrical conductivity of the fluid has two immediate consequences:

- i) the induced currents $\sigma(\mathbf{U} \times \mathbf{B})$ are much less than those due to the applied electrical field,
- ii) the external applied current will penetrate into the liquid only on a short distance and will rapidly decay in y -direction.

The applied fields then give a Lorentz force

$$\mathbf{F} = \sigma \mathbf{E} \times \mathbf{B} = F_x \cdot \mathbf{e}_x \quad (4)$$

which has a streamwise component only. Such Lorentz force was calculated by Grienberg [8] using a series expansion to determine the electromagnetic field distributions assuming a periodical dependence in z -direction.

He found that in a good approximation the resulting force decays exponentially with y :

$$F_x = 2.87 j_0 B_0 e^{-\pi y / (2a)} \quad (5)$$

where a denotes the spacing of electrodes and magnetic poles, j_0 and B_0 the applied electric current density and external magnetic field induction, respectively. Equal spacing of electrodes and magnetic poles gives a maximum force density for given j_0 and B_0 .

As done by Tsinober & Shtern [5], the force (5) can be inserted in the boundary layer equations for a flat plate. In the non-dimensional form of the boundary layer equations then appears a characteristic parameter, the Hartmann number

$$Ha^2 = \frac{j_0 B_0 a^2}{\rho \nu U_0}, \quad (6)$$

that describes the ratio of electromagnetic to viscous forces. Provided a certain value of the Hartmann number, the boundary layer reaches an asymptotic thickness, i.e. the velocity component normal to the plate becomes equal to zero. That means, the momentum loss due to friction is just balanced by

the momentum gain due to the applied Lorentz force. Under these circumstances an exponential boundary layer profile

$$\frac{U_x}{U_0} = 1 - e^{-\pi y/(2a)} \quad (7)$$

comparable to the asymptotic suction profile develops. The exponential profile is much more stable than the usual Blasius boundary layer [9]. Therefore it is possible with a suitable chosen Hartmann number to keep the boundary layer in the laminar state even for higher Reynolds numbers. This leads to a significant reduction of the skin friction compared to the pure hydrodynamic case. It is interesting to note, that the characteristic parameters of the exponential profile (7), i.e. displacement thickness, momentum thickness and shape parameter are only functions of the electrode and magnetic pole spacing a .

Rough estimates of the net effect of boundary layer stabilization on the friction losses were done by Gailitis and Lielausis [4]. They estimate a possible net gain of this approach with respect to the energetical balance taking into account the efforts for the electromagnetic fields. There were first demonstration experiments by Nerets and Shtern [10] which qualitatively have shown the effect. However, much more data are necessary for a profound understanding of the fluiddynamic phenomena. A difficulty for proving the predicted boundary layer properties is that an ideally uniform force distribution as described by (5) can not be obtained by such a simple configuration of magnets and electrodes as sketched in Fig. 1. In reality there is an additional periodic variation of the Lorentz force in z -direction.

3 Experimental arrangement

For a first validation experiment we designed a rotating annular tank. A sketch of this tank is shown in Fig. 2. The tank itself is made from Plexiglas to make flow visualization possible. Also this material does not corrode, a serious point for experiments with electrolytes. The inner radius of the tank is 355 mm, the cross section 100 mm \times 100 mm. A small DC motor drives the channel directly at its outer radius by a rubber covered wheel. Modifying the driving voltage of this engine and choosing wheels of different diameters, one can adjust the rotation speed of the angular channel between 1 and 3 rpm. The speed is controlled by a speedometer and corresponds to a fluid velocity range from 0.037 m/s to 0.113 m/s in the middle of the channel cross section.

The diameter of the tank is large enough so that most of the vorticity created by our experimental body decays during one revolution of the tank. Without a testbody inserted in the channel, the fluid follows a solid body rotation after approximately 3 minutes from startup.

20 liters of a solution of 10% Copper sulphate CuSO_4 and 5% sulphuric acid H_2SO_4 in water are used as the test fluid. This solution has a density of 1120 kg/m^3 and gives a conductivity of 16 S/m, the kinematic viscosity is nearly equal to that of water. Besides of its 4 times higher conductivity this solution has several other advantages compared to salt water for laboratory use:

provided a critical current density is not exceeded, no electrolytical bubbles are produced at the copper electrodes and the process of electrolytic corrosion of the copper anodes can be canceled simply by reversing the voltage, so the former anodes are renewed by galvanic copper deposition.

The colour of the solution is a deep blue, so we used as a marker for the flow visualizations Potassium permanganate KMnO_4 dissolved in a small volume of the solution. This gives a very dark violet marker with matched density. Alternatively aluminum particles distributed on the free surface of the fluid were used to visualize the flow.

4 Control of boundary layer separation

Control of the cylinder wake and, in particular, control of the boundary layer separation on the cylinder surface shall be performed by a specific array of electrodes and permanent magnets. The straightforward application of the flat plate array of Fig. 1 to the circular cylinder is sketched in Fig. 3. The Lorentz force is mainly directed parallel to the cylinder surface. One could imagine two plates as shown in Fig. 1 each wrapped around a half cylinder, so that the Lorentz forces on both sides have the same direction. Depending on the polarity of the applied electric field the force sketched by the bend arrows can be directed with the mean flow velocity or opposite to it.

The mechanism allowing to prevent the separation of the boundary layer from the cylinder surface is again to add momentum into the fluid region near the cylinder surface. Separation occurs, when fluid decelerated by friction forces is exposed to an adverse pressure gradient stronger than the remaining kinetic energy of the fluid. Increasing the near wall fluids energy by accelerating it with the Lorentz forces up to a velocity where it can withstand the pressure gradient should therefore lead to separation suppression.

Our cylinder has a diameter of 2 cm, a wetted length of 9 cm, the electric and magnetic poles are 4 mm in width, therefore the electrode and magnet pole spacing is $a = 4$ mm. The small “nose” shown in the view on the circular cross section of the cylinder in Fig. 3 contains the current supplies for the electrodes. The magnetic induction between the magnetic poles is $B_0 = 0.2$ T, a maximum current density of 2000 A/m^2 at the electrodes can be supplied.

Figure 4 shows the effect of an applied Lorentz force directed downstream, the bend white arrow denotes the direction of the electromagnetic force. This force is generated on both sides of the cylinder by an applied voltage of 0.56 V resulting in a current density of 1027 A/m^2 . The value of the corresponding interaction parameter N , the ratio of electromagnetic to inertial forces $j_0 B_0 D / (\rho U_0^2)$ is 2.54. The picture is taken at a Reynolds number of 760 corresponding to a mean flow velocity of 3.8 cm/s, so without the applied force one would have a well developed von Kármán vortex street behind the cylinder as shown as a reference in Fig. 5. Instead the dye streaks are smooth and not deformed by vortices. So by suppressing unsteady separation, the von Kármán vortex street is suppressed. The flow can be maintained in this stage as long as the current density with the specified value is applied to the electrodes.

A strong enough downstream forcing results in a jet originated at the rear stagnation point. This jet, indicated by the particle traces in Fig. 6, exerts a net force on the cylinder driving it upstream, the global effect of the electromagnetic forces is now production of thrust. The Lorentz force is denoted by the two white bend arrows on the cylinders back side. The parameters of the depicted scene are 3.8 cm/s mean flow velocity, i.e. a Reynolds number of 760, an applied voltage of 1.03 V, a current density j_0 of 1861 A/m² and a resulting interaction parameter N of 4.6. Looking at the length of the particle traces, one can estimate the velocity inside the jet as two to three times this of the mean flow. Note that there is a velocity gradient in the mean flow from the top to the bottom of Fig. 6 due to the rotating channel motion. The flow is steady, provided that a constant current density is supplied.

In Fig. 7 the Lorentz force sketched by the bend white arrow is directed upstream on both sides of the cylinder due to the opposite current direction. This force direction accelerates the fluid in the boundary layer opposite to the mean flow. The picture is again taken at a Reynolds number of 760 with the same parameters as Fig. 4 except for the sign of the voltage and shows the flow in the stage just after applying the force. Two symmetric vortices are formed similar to those observed on a cylinder starting from the rest [11]. In contrast to this case, the separation points are strongly shifted towards the forward stagnation point. In the steady state a von Kármán vortex street with larger vortices and higher transverse extension compared to the usual case forms.

The same observations can be made for Reynolds numbers up to 2200, corresponding to the highest possible speed in our facility.

5 Numerics

The limitation of Re to quite low values in our experiment gives, on the other hand, the possibility of performing direct numerical simulations of the flows. This is done here by using a finite difference algorithm in a vorticity streamfunction formulation, for more details of the numerics see [1]. This code solves the two dimensional Navier–Stokes equations

$$\frac{\partial \mathbf{v}}{\partial t} + (\mathbf{v} \cdot \nabla) \mathbf{v} = -\nabla p + \frac{2}{Re} \Delta \mathbf{v} + \frac{N}{2} \mathbf{f} \quad (8)$$

$$\nabla \cdot \mathbf{v} = 0 \quad (9)$$

The factor of two in the terms with N and Re in Eq. (8) is due to the fact that the equations are based on the cylinder radius as the characteristic length, whereas the nondimensional parameters Re and N are defined as usual with the cylinder diameter D , i.e.

$$Re = \frac{U_0 D}{\nu}, \quad N = \frac{j_0 B_0 D}{\rho U_0^2}. \quad (10)$$

The interaction parameter N gives the ratio of the electromagnetic forces to the inertia forces. The problem is formulated in cylinder coordinates, the mesh extends over 121 points in radial and 121 points in azimuthal direction. The grid is linear in azimuthal direction and exponentially spaced ($r_i \sim$

$e^{\gamma i}$) in radial direction, where i is the index and γ denotes a scaling factor. The grid extends to 50 cylinder radii, due to the exponential spacing in r a sufficient resolution of the boundary layer for the chosen Reynolds number of 200 is obtained.

We describe the Lorentz force in (8) by the simple relation

$$\mathbf{f} = e^{-\alpha(r-1)}g(\theta)\mathbf{e}_\theta \quad \text{with} \quad \begin{array}{ll} g = 1 & : \quad 5^\circ \leq \theta \leq 175^\circ \\ g = -1 & : \quad 185^\circ \leq \theta \leq 355^\circ \\ g = 0 & : \quad \text{elsewhere} \end{array} \quad (11)$$

accounting for the slots at the front and rear stagnation points where no electrodes are present. The neglect of any radial force component and the constant radial dependence for each angle θ represents, obviously, a simplification of the real experimental situation.

The value α describes the electromagnetic penetration into the liquid which is mainly defined by the electrode spacing, modeled in correspondence to the experimental situation by $\alpha = 5\pi/4$. The interaction parameter as given in (10) contains the square of the velocity in the denominator. In order to characterize the electromagnetic action for constant external velocities it is useful to introduce the quantity

$$S = N \cdot Re^2 = j_0 B_0 \frac{D^3}{\rho \nu^2}. \quad (12)$$

which is independent of U_0 .

Figure 8 shows calculations of the flow field for different values of S . The streamlines have equal values for all presented figures. Only a small part of the region covered by the mesh is shown. In these figures the flow goes always from left to right. In the top part of Fig. 8 the case of flow without any electromagnetic forcing is shown. The flow is unsteady and shows the characteristic features of the von Kármán vortex street at a Reynolds number of 200, i.e. appropriate values of the Strouhal number and the drag and lift coefficients. For a small electromagnetic forcing of $S = 8 \cdot 10^4$ corresponding to a current density of 17.4 Am^{-2} one can see an interesting modification of the flow. Though it is still unsteady, the separation direct at the wall disappears. Instead separation takes place in the fluid region near the wall. Behind the cylinder a region with two relatively stable recirculation bubbles forms, wherein the fluid motion is rather slow. From this region vortices are shed with approximately the Strouhal frequency but considerably smaller extension compared to the force free case. Further increase of S leads to the third picture from above of Fig. 8. Separation is fully suppressed by the applied force, additionally a slight acceleration of the fluid takes place, as can be seen from the narrowing of the streamlines behind the cylinder. Under these conditions, i.e. $Re = 200$, $S = 2 \cdot 10^5$ and therefore $N = 5$, the flow is stable. The main part of the fluid is accelerated during it's way from the stagnation point over the first half of the cylinder surface. Most of this accelerated fluid leaves the cylinder tangentially at approximately 100° , respective -100° , forming two jets which meet at one cylinder diameter downstream. Embedded between these jets is a region of lower velocity. At a very high surface force $S = 2 \cdot 10^6$ the cylinder acts mainly as a thrust generator. The

accelerating effect on the fluid is not only obvious in the region behind the cylinder, but also in front of the cylinder the streamlines are considerably narrowed. The two jets originate now from 135° and meet at 0.5 cylinder diameters behind the rear stagnation point, forming a strong jet which already shows a jet instability. In the region between the two tangential jets recirculation takes place and forms several small vortices.

Figure 9 shows profiles of the mean streamwise velocity over y/D at two locations behind the cylinder with different distances to the coordinates origin in the cylinders mid point. The values for the applied force S are rather low, so that for the curves with $S = 4 \cdot 10^4$ and $S = 8 \cdot 10^4$ values of the stationary solution are shown.

In the bottom part of Fig. 9, depicting the conditions at a distance of 0.5 diameters behind the rear stagnation point, the tendency of the flow to form two distinct jets can clearly be seen. With increasing force S the distance between these jets narrows and their velocity increases. At the lower surface force values, i.e. $S = 4 \cdot 10^4$ and $S = 8 \cdot 10^4$ regions of recirculating fluid embedded between the two jets and the y axis can be seen. The velocity at the y axis is larger than zero, indicating that the fluid very near the cylinder surface leaves the cylinder only at the rear stagnation point, i.e. there is a small boundary layer at the cylinder which does not separate. For the case with the highest surface force $S = 2 \cdot 10^5$ presented in Fig. 9, almost no recirculation is found. The velocity profiles 7 diameters downstream of the rear stagnation point have smaller gradients due to dissipation. That one for $S = 4 \cdot 10^4$ shows a characteristic wake profile, whereas the influence of the two jets on the shape of the other profiles still exists. The profile belonging to $S = 8 \cdot 10^4$ is formed by a wake shape bounded by two distinct velocity maxima. The momentum surplus contained in the two jets is higher than the wake defect. Looking at the curve corresponding to $S = 2 \cdot 10^5$, the two jets have joined forming a single jet with a relatively broad velocity maximum.

Figure 10 gives the vorticity and pressure distributions on the cylinder surface along one half cylinder where the angle θ goes from the front to the rear stagnation point. The vorticity distribution shows again that for the considered values of the surface force S separation is suppressed as indicated by the always positive sign of the vorticity on the cylinder surface. Increase of the surface force leads to an increasing vorticity. The reason is obvious, due to the exponential distribution of the force (11) the main part is concentrated very near the wall. Higher values of S therefore result directly in a steeper gradient of the velocity profile at the wall causing higher vorticity. Pressure distributions over the cylinder surface given in the bottom part of Fig. 10 are normalized with the stagnation point pressure $\rho \cdot U_0^2/2$. The pressure distribution for $S = 4 \cdot 10^4$ is only slightly different from that of the non forced case. The minimum value is lower caused by the accelerated fluid, and the pressure at the rear stagnation point is higher due to the reduction of the recirculation region. With increasing surface force, the minimum of the pressure distribution reaches lower and lower values and the pressure at the rear stagnation point increases. Note that at $S = 2 \cdot 10^5$ the pressure value at the rear stagnation point surpasses the value of the front stagnation point, i.e. there is a net force opposite to the mean flow direction due to the pressure difference between front and rear stagnation points.

The evolution of the coefficients of pressure drag, friction drag and total drag with the applied surface force at a Reynolds number of 200 is shown in Fig. 11. It summarizes some of the flow features observed in the previous diagrams. With increasing surface force the friction drag increases. This is due to the increasing wall friction resulting from the steeper velocity gradient at the wall. The form drag decreases with increasing surface force because of separation suppression. At sufficient high values of the surface force a jet originates from the rear stagnation point causing there a higher pressure than at the front stagnation point. Therefore the form drag coefficient even reaches negative values. The total drag coefficient c_D taken as the sum of c_F and c_P decreases first with increasing surface force and increases then due to the growing influence of the wall friction on the drag coefficient. However, taking into account the momentum added to the fluid by applying the body force, we have a net thrust even for low surface force values.

6 Practical Significance/Usefulness

Drag reduction of marine vehicles will result in longer operation ranges, increased speed, higher payload, or reduced fuel cost. The application of laminar boundary layer theory to the flow over a flat plate equipped with suitable magnets and electrodes indicates the possibility to reduce friction drag by keeping the boundary layer in its laminar state at Reynolds numbers, where it otherwise would be turbulent.

In the present paper the focus lies mainly in the application of the Lorentz force to suppress separation. Main result is that a quasilaminarized flow without vortex shedding around a circular cylinder can be attained by means of electromagnetic forces. Further consequences are the reduction of form drag, and the possibility of maintaining or creating a lift force on the body by a suitably chosen Lorentz force distribution.

7 Discussion

We presented first results from flow visualizations and numerical calculations on active control of the flow around a cylinder by means of electromagnetic forces. The principal feasibility of this approach has clearly been demonstrated, both experimentally and numerically.

Detailed experimental investigations of the flow field and the forces acting on the cylinder are the subject of our next steps. For this purpose the rotating channel apparatus should be replaced by a water tunnel in order to obtain reliable quantitative results. Besides a variation of the supplied surface force, also their extension into the fluid and their homogeneity has to be varied and optimized by investigation of test bodies with different configurations of electrodes and magnets.

Because the value of the body force is a function of the applied current density, it is easy to change this force in time. This makes it possible to influence the unsteady flow itself instead changing its nature into the steady state to

achieve certain goals. This approach may be more effective from the economical point of view than the “brute force way” of total relaminarization. Several experiments done with conventional methods like periodic blowing and suction or cylinder rotation could be approximately duplicated by the use of appropriate configured electromagnetic force fields.

8 Acknowledgment

Financial support from “Deutsche Forschungsgemeinschaft” under grant INK 18/A1-1 is gratefully acknowledged. The cooperation with the Riga Institute was supported from the German Ministry of Research and Technology.

NOMENCLATURE

a	spacing of electrodes and magnets, m
\mathbf{B}	magnetic induction, T
c_D	total drag, dimensionless
c_F	frictional drag, dimensionless
c_P	pressure drag, dimensionless
D	cylinder diameter, m
\mathbf{E}	electric field vector, V/m
\mathbf{e}	unity vector, dimensionless
\mathbf{F}	force density, N/m ³
\mathbf{f}	force density, dimensionless
g	factor, dimensionless
Ha	Hartmann number, dimensionless
\mathbf{j}	current density, A/m ²
N	Interaction parameter, dimensionless
p	pressure, dimensionless
r	radius, dimensionless
Re	Reynolds number, dimensionless
S	surface force, dimensionless
t	time, dimensionless
\mathbf{U}	flow velocity, m/s
\mathbf{v}	flow velocity, dimensionless
x, y, z	Cartesian coordinates, m

Greek Symbols

α	force penetration depth, dimensionless
γ	proportional factor
θ	angle, degrees
ν	kinematic viscosity, m ² /s
ρ	density, kg/m ³
σ	conductivity, S/m
ω	vorticity, dimensionless

Subscripts

0	imposed quantity
i	index
max	maximum
r	radial direction
x, y, z	direction (Cartesian coordinates)
θ	azimuthal direction

Operator Symbols

∇	Nabla vector operator
\cdot	inner product
\times	cross product

References

- [1] Mutschke, G., Shatrov, V. & Gerbeth, G., Cylinder Wake Control by Magnetic Fields in Liquid Metal Flows, this volume, 1997.
- [2] Meng, J.C.S., Major Engineering Physics for Optimization of the Seawater Superconducting Electromagnetic Thruster, in *Progress in Astronautics and Aeronautics (AIAA-Report)*, Branover, H., Unger, Y., Eds., Vol.148, pp.183–208, AIAA Inc., Washington DC, 1990.
- [3] Motora, S. and Takezawa, S., Development of MHD Ship Propulsion and results of sea trials of an experimental ship YAMATO–1, 2. Int. Conf. on Energy Transfer in MHD Flows, Aussois, France, pp.501–510, September 1994.
- [4] Gailitis, A. and Lielausis, O. , On a possibility to reduce the hydrodynamical resistance of a plate in an electrolyte, in *Applied Magneto-hydrodynamics. Reports of the Physics Institute 12*, (Prikladnaya Magnitogidrodinamika. Trudy Instituta Fiziki, 12), Riga, pp. 143–146 (in Russian), 1961.
- [5] Tsinober, A. B. and Shtern, A. G., On the possibility to increase the stability of the flow in the boundary layer by means of crossed electric and magnetic fields, *Magnitnaya Gidrodinamica*, No.2, pp.152–154 (in Russian) 1967.
- [6] Henoach, C. and Stace, J., Experimental investigation of a salt water turbulent boundary layer modified by an applied streamwise magnetohydrodynamic body force, *Phys. Fluids*, Vol.7, No.6, pp.1371–1383, 1995.
- [7] Nosenchuck, D., Culver, H. and Brown, G., Volumetric Boundary Layer Characteristics of EMTC, *Bulletin of the APS*, Vol.40, No.12, p.1988, 1995.
- [8] Grienberg, E., On determination of properties of some potential fields, in: *Applied Magneto-hydrodynamics. Reports of the Physics Institute 12*, (Prikladnaya Magnitogidrodinamika. Trudy Instituta Fiziki, 12), Riga, pp.147–154 (in Russian), 1961.
- [9] Drazin, P.G. and Reid, W.H., *Hydrodynamic stability*. Cambridge Monographs on Mechanics and Applied Mathematics, Cambridge University Press, 1981.
- [10] Nerets, Y. and Shtern, A., Experimental investigation of a possibility to increase the stability of flow in the boundary layer, 6-th Riga MHD Conf. Riga, pp.85–87 (in Russian), 1968.
- [11] Coutanceau, M. and Defaye, J.,R., Circular cylinder wake configurations: A flow visualization survey, *Appl Mech Rev*, Vol 44, No 6, pp.255–305, 1991.

List of Figures

- Figure 1 Sketch of the electric (thin) and magnetic (thick) fieldlines and the resulting Lorentz force (gray arrow) over a flat plate
- Figure 2 Schematic diagram of the experimental set-up
- Figure 3 Sketch of the cylinder equipped with electrodes and magnets. The right side shows the opposite electric field polarity resulting in an opposite direction of the Lorentz force.
- Figure 4 Experimental visualization of electromagnetic downstream forcing resulting in separation suppression.
- Figure 5 Experimental visualization of the original von Kármán street.
- Figure 6 Experimental visualization of strong electromagnetic downstream forcing resulting in a jet flow from the rear stagnation point.
- Figure 7 Experimental visualization of electromagnetic upstream forcing resulting in early separation at the front region.
- Figure 8 Streamlines for the flow around a cylinder with different electromagnetic forces S , $Re=200$.
- Figure 9 Stationary velocity profiles $v_x(y/D)$ for $x/D = -7.5$ (top figure) and $x/D = -1.5$ downstream (bottom figure), $Re=200$.
- Figure 10 Vorticity and pressure distribution on the cylinder surface for different surface forces S , $Re=200$.
- Figure 11 Drag coefficients (frictional c_F , pressure c_P , total c_D) over S for $Re=200$.

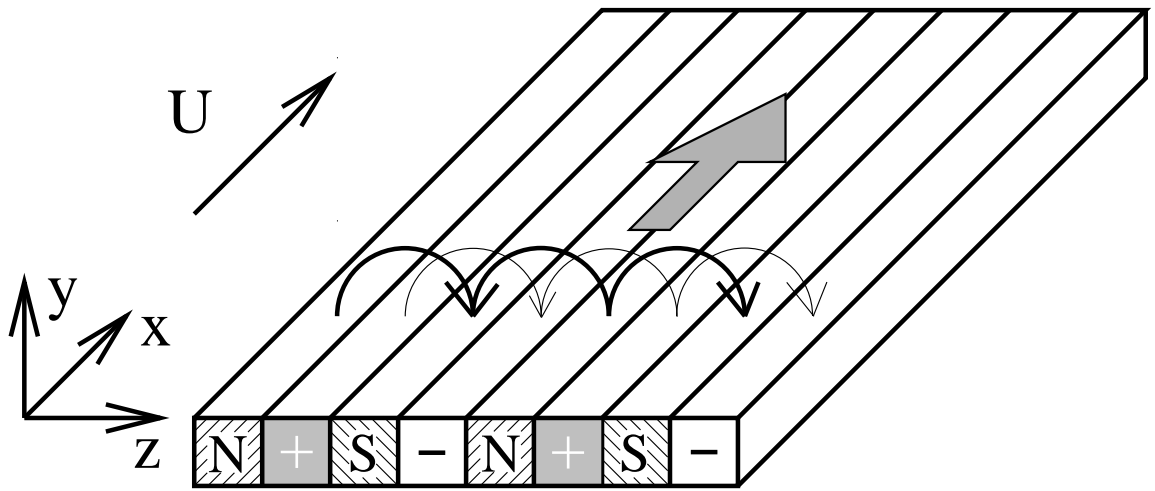


Figure 1: Weier/Gerbeth/Mutschke/Platacis/Lielausis

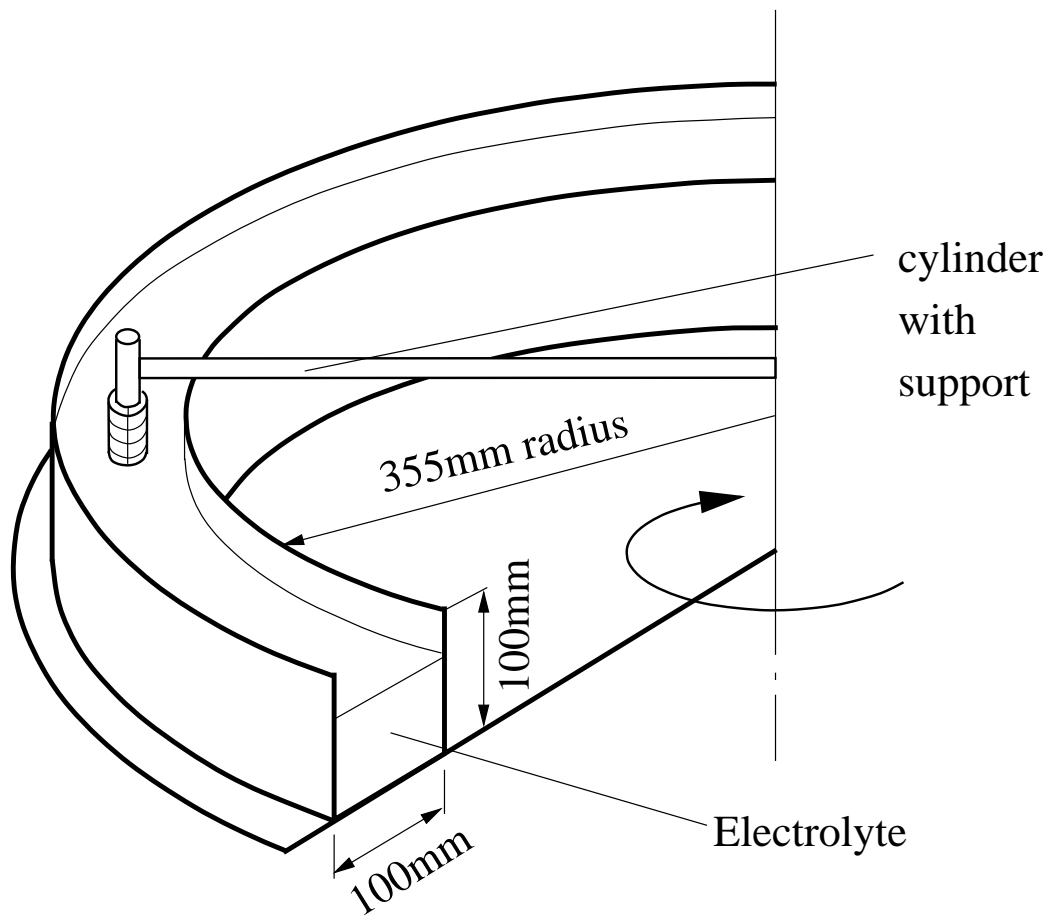


Figure 2: Weier/Gerbeth/Mutschke/Platacis/Lielausis

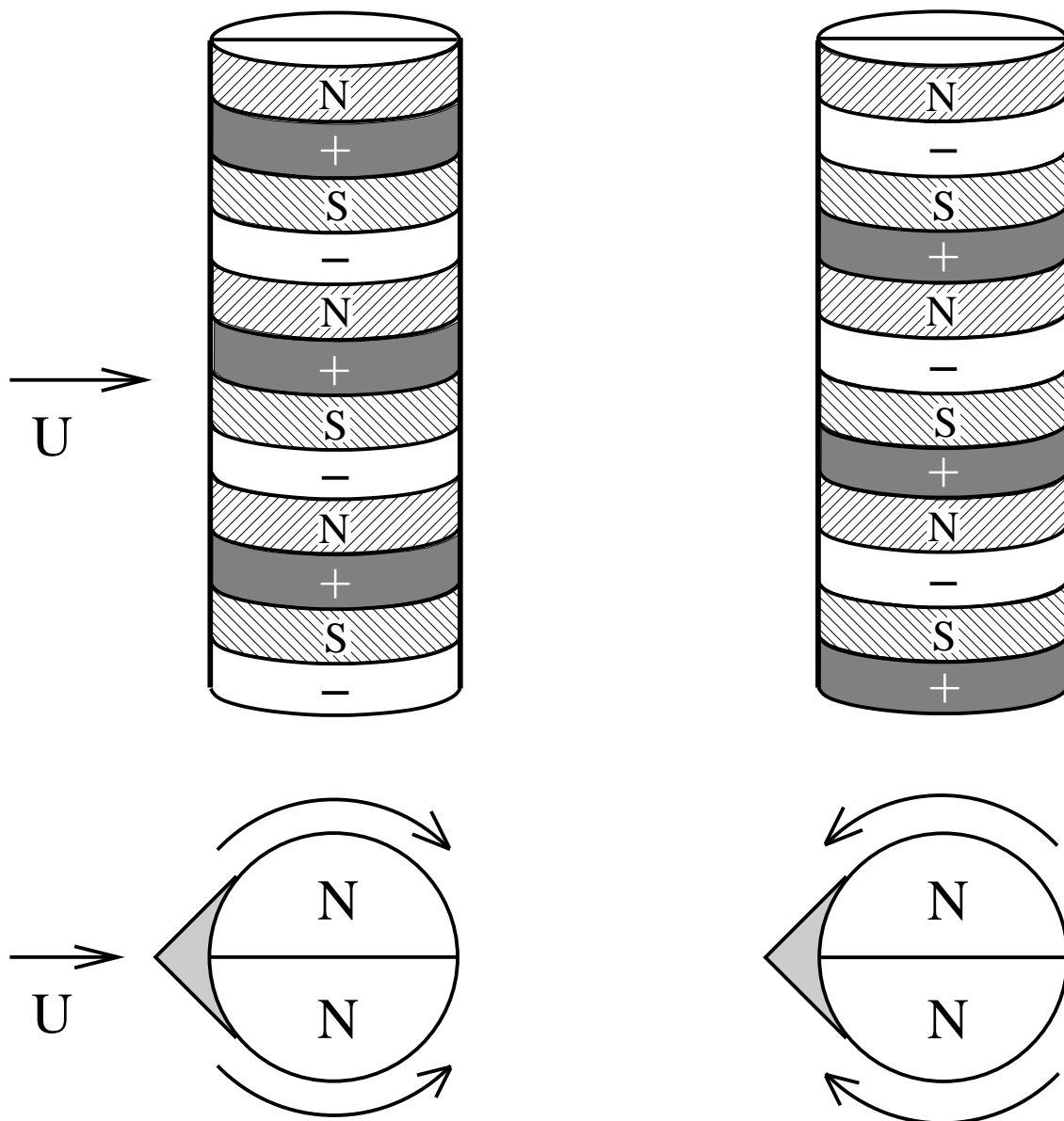


Figure 3: Weier/Gerbeth/Mutschke/Platacis/Lielausis

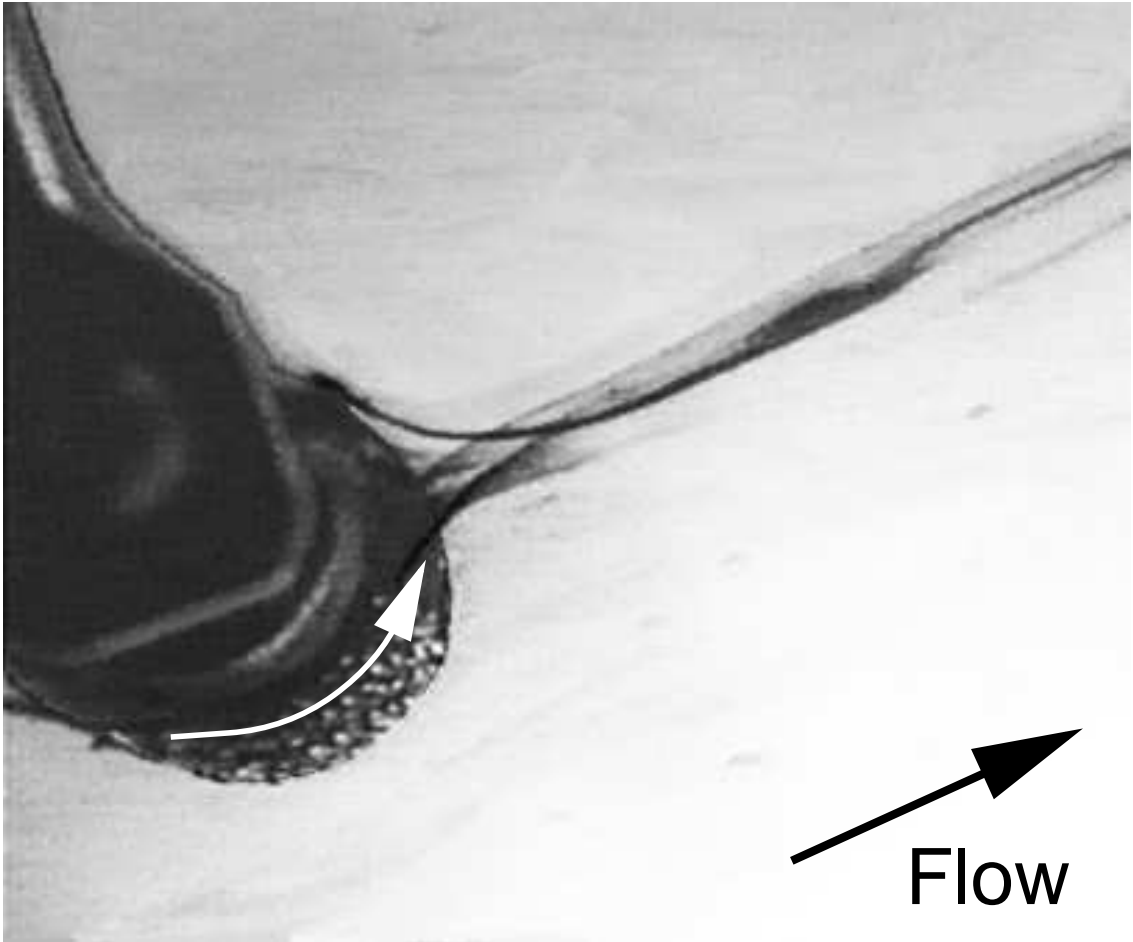


Figure 4: Weier/Gerbeth/Mutschke/Platacis/Lielausis

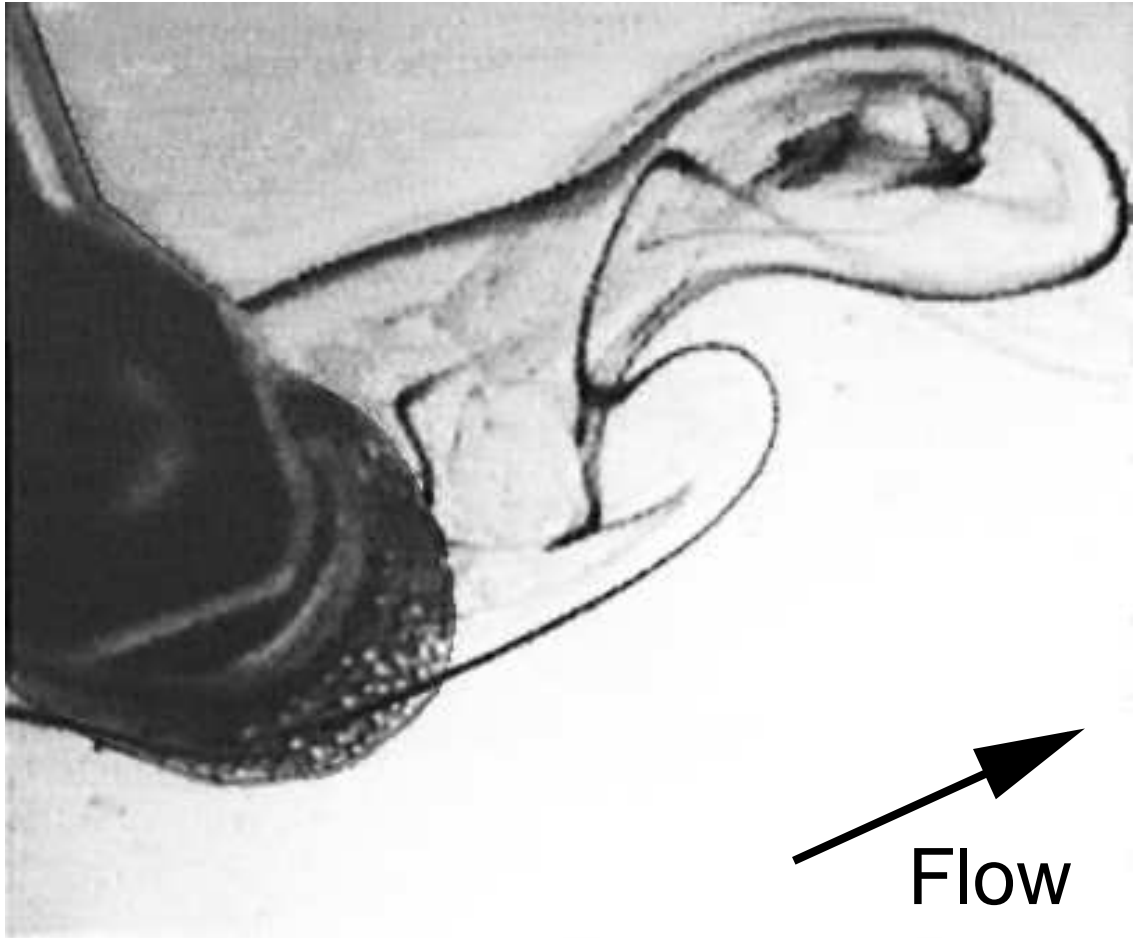


Figure 5: Weier/Gerbeth/Mutschke/Platacis/Lielausis

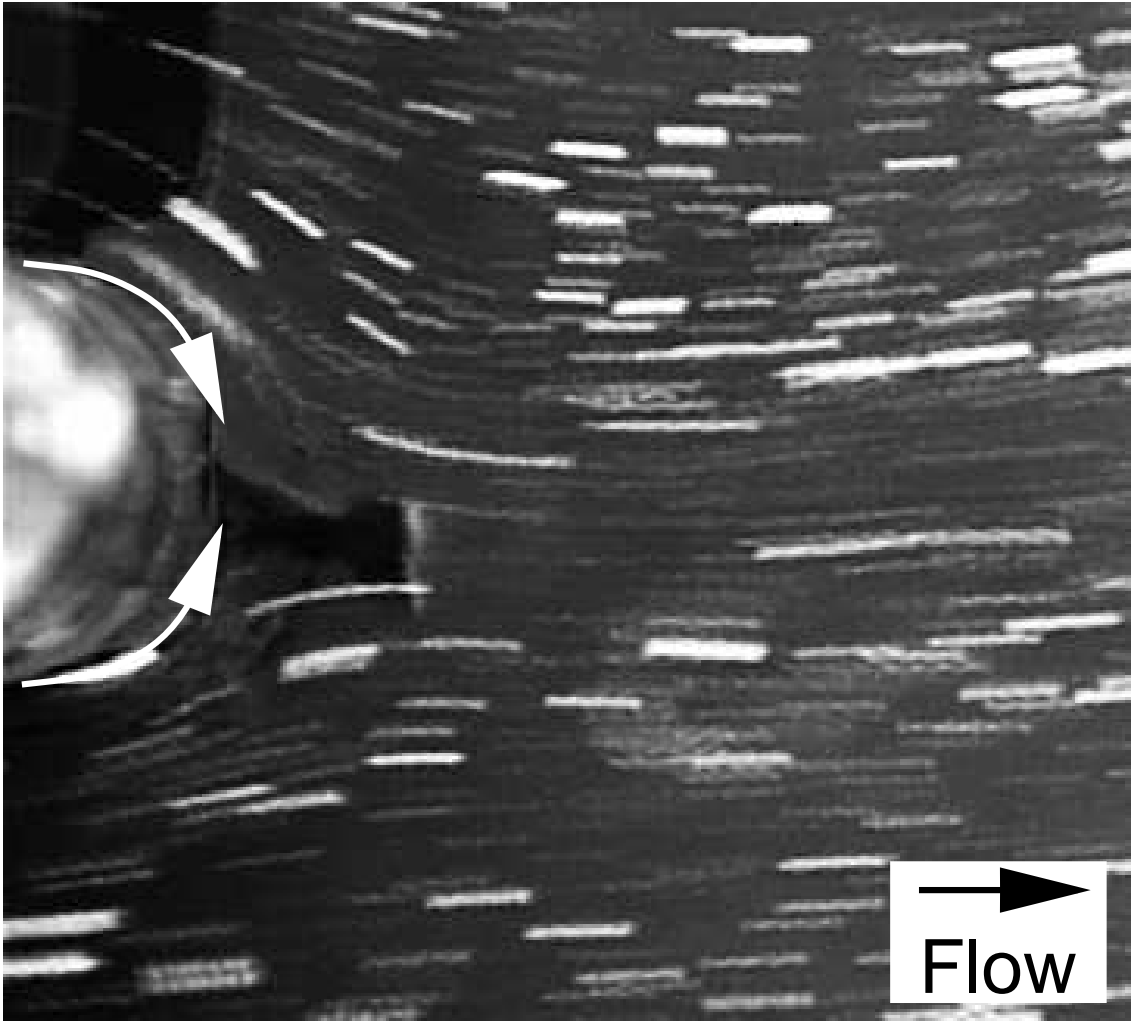


Figure 6: Weier/Gerbeth/Mutschke/Platacis/Lielausis

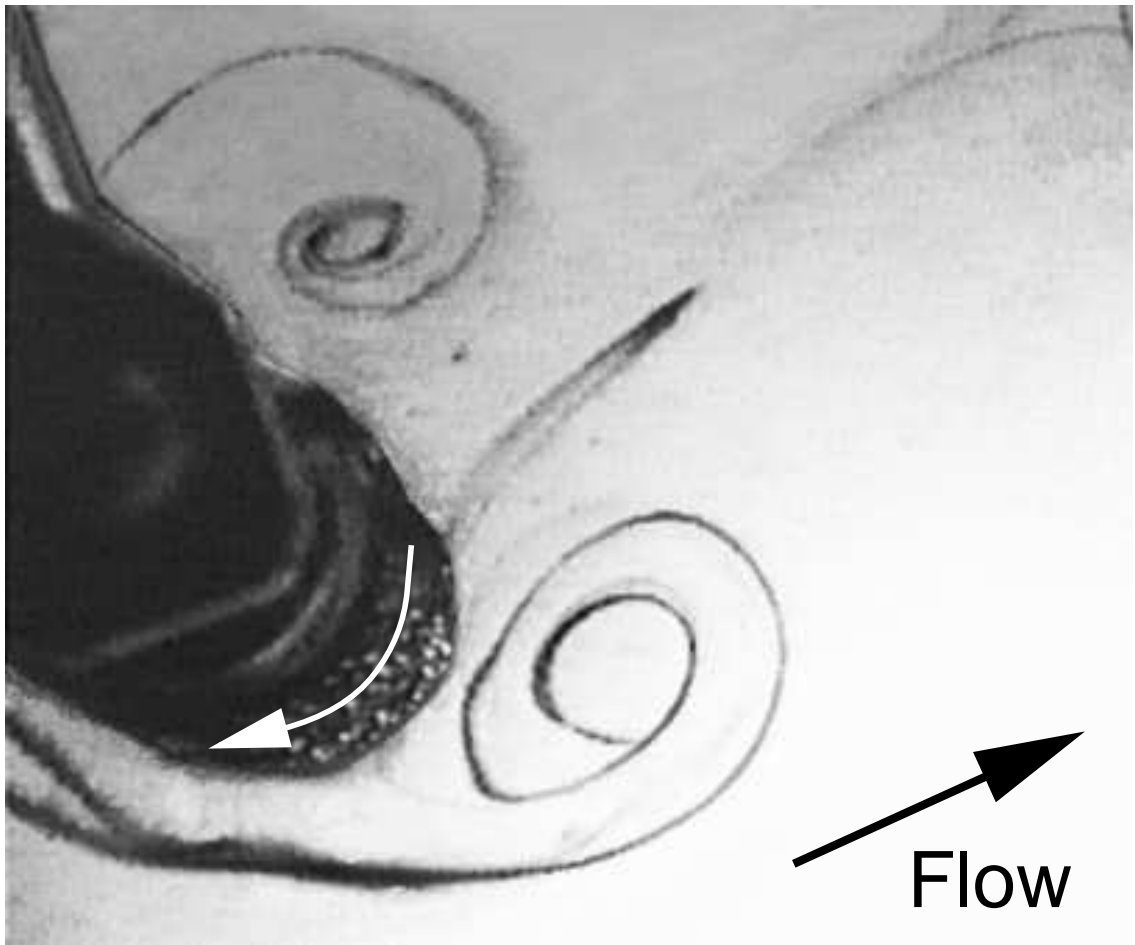


Figure 7: Weier/Gerbeth/Mutschke/Platacis/Lielausis

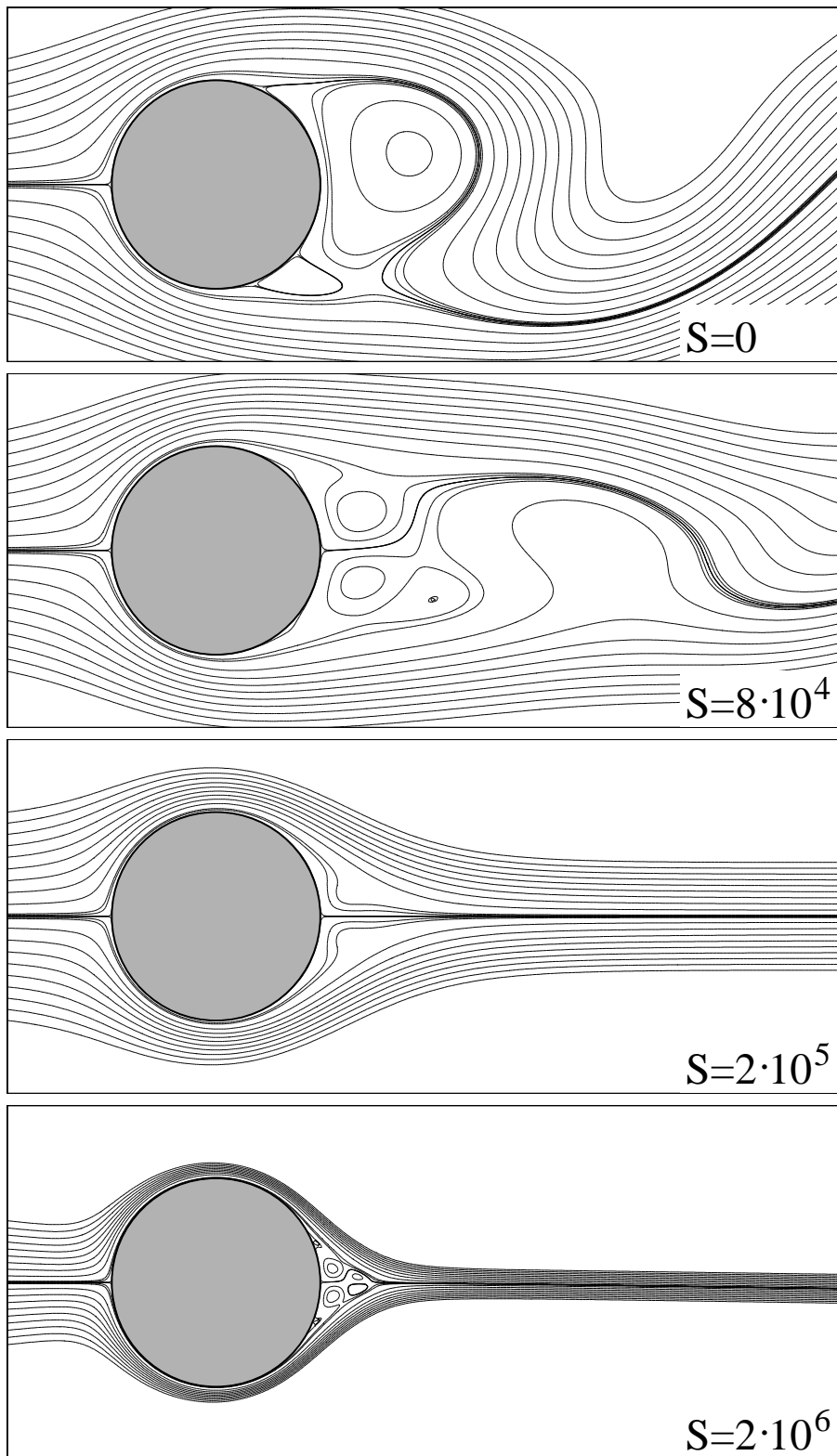


Figure 8: Weier/Gerbeth/Mutschke/Platacis/Lielausis

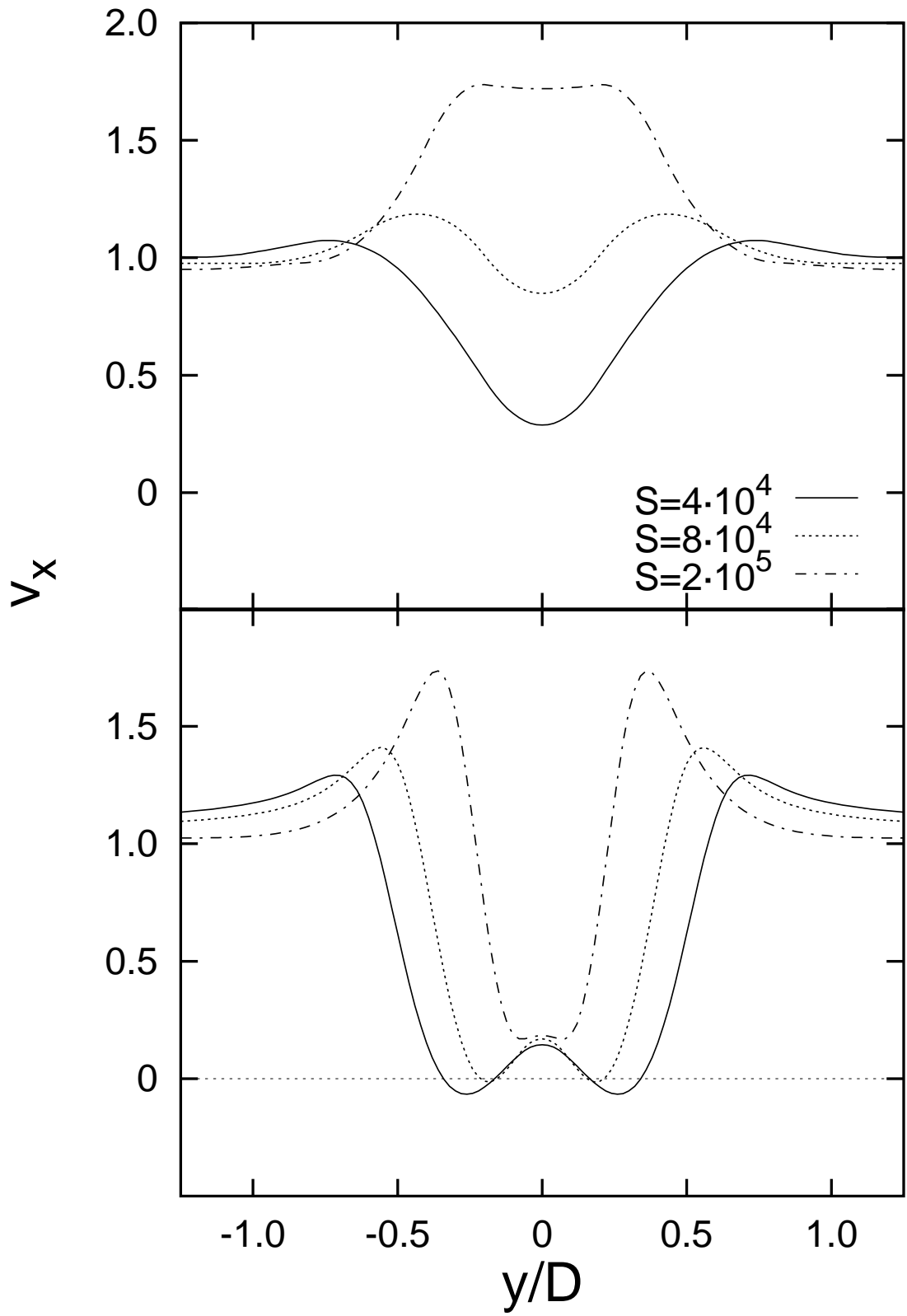


Figure 9: Weier/Gerbeth/Mutschke/Platacis/Lielausis

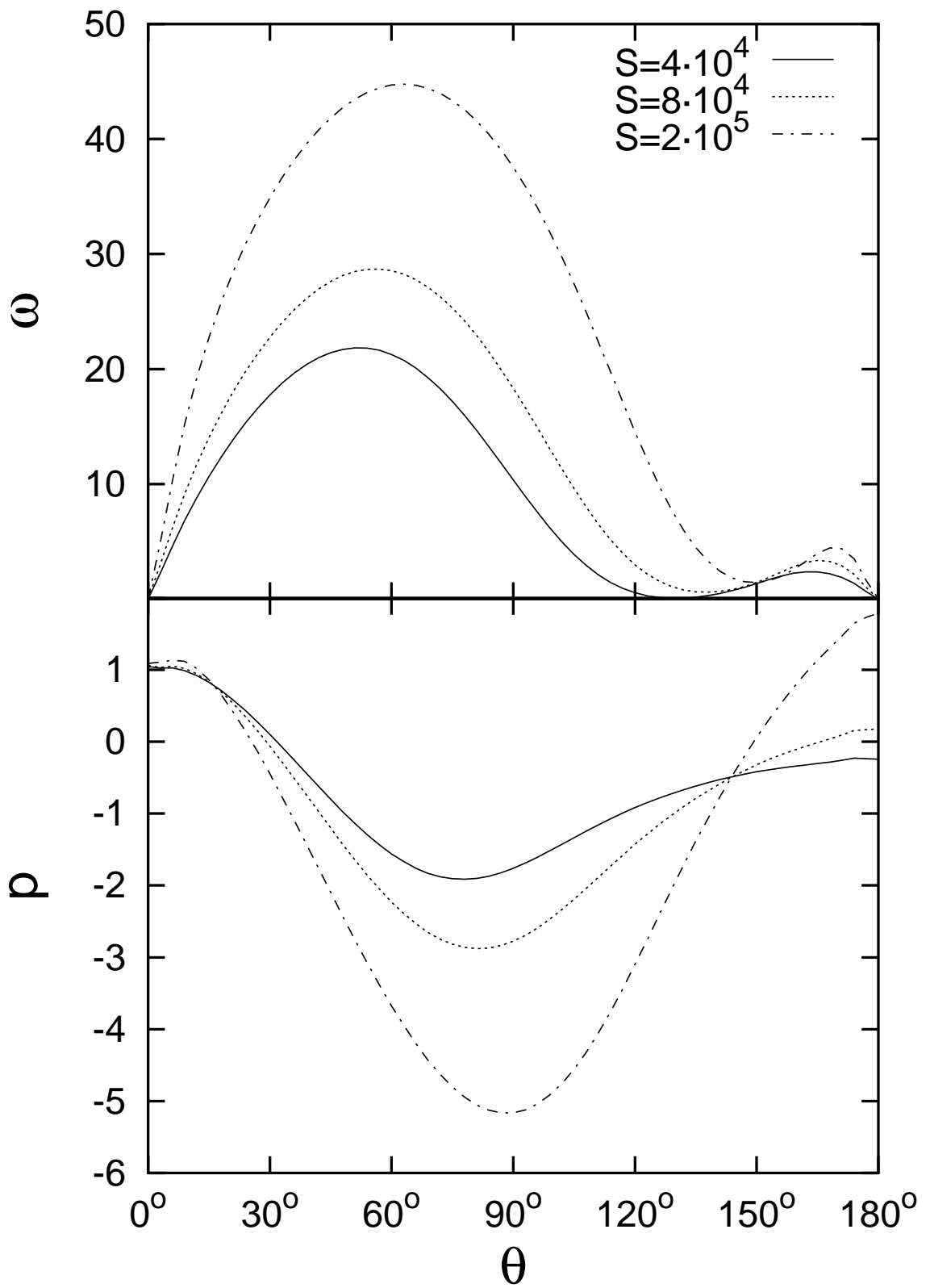


Figure 10: Weier/Gerbeth/Mutschke/Platacis/Lielausis

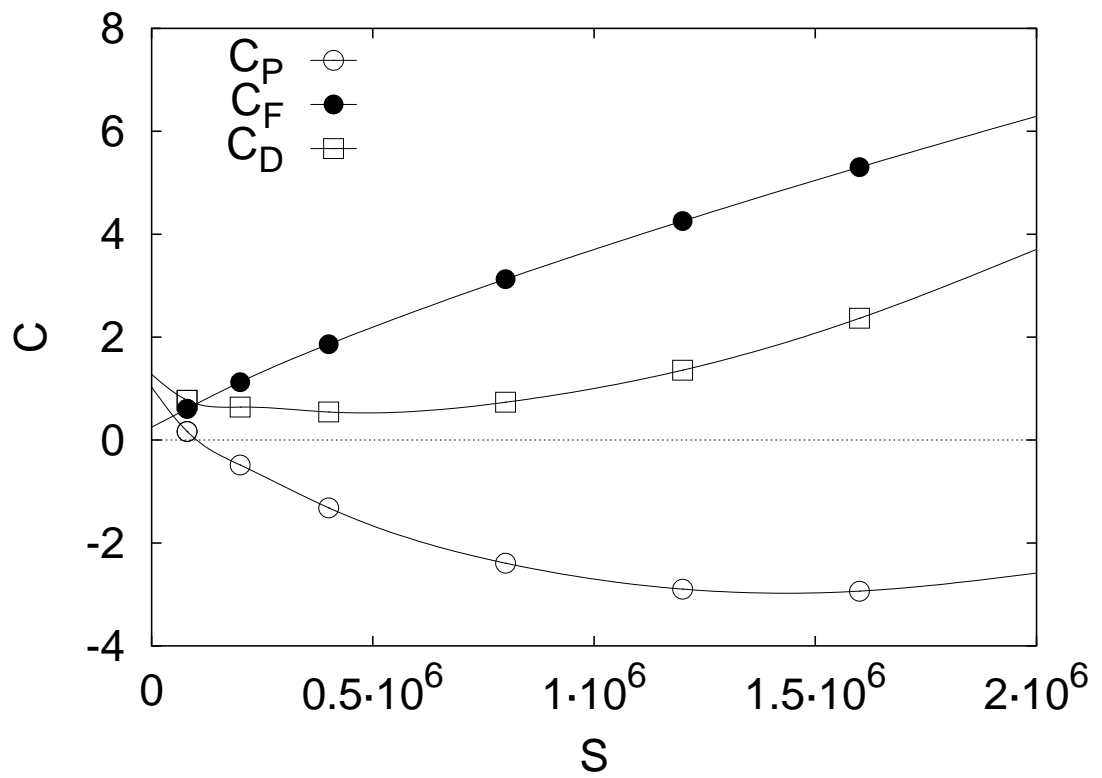


Figure 11: Weier/Gerbeth/Mutschke/Platacis/Lielausis